AIAA JOURNAL
Vol. 39, No. 6, June 2001

Experimental Investigation of Two-Stream Mixing Flow with Multiple Tabs

S. C. M. Yu* and P. K. Koh†
Nanyang Technological University, Singapore 639798, Republic of Singapore

Vortex-generating tabs arranged in the form of an array have been examined experimentally using a laser Doppler anemometer in a two-stream mixing flow situation. The vortex-generating tabs are the "delta tabs," i.e., triangular-shaped protrusions into the flow attached to the trailing edge of the splitter plate. A velocity ratio of 2:1 (upper and lower) between the two coflowing streams was used. Three arrangements for the tabs are investigated. Case 1 has all of the tabs located on the high-speed side. The tabs are located alternatively on either side of the splitter plate for case 2, and finally, case 3 is similar to case 2, but the tab on the low-speed side is tilted upstream (i.e., similar to a delta-wing vortex generator). Mutual cancellation between streamwise vortices rotating in the opposite sense was observed in case 1, whereas in case 2 the merging of streamwise vortices rotating in the same sense had delayed the decay of the streamwise vorticity. For case 3 the upstream tilted tab appeared to have generated relatively weak streamwise vortices so that they were canceled off by the vortices generated on the high-speed side near the trailing edge. Finally, the turbulence characteristics for each case are presented and discussed.

Nomenclature

H	=	boundary-layer shape factor, δ^*/Θ
h_{tab}	=	tab height
k	=	turbulent kinetic energy, $\frac{1}{2}(u'^2+v'^2+w'^2)$
Re	=	Reynolds number, $U_r h_{\text{tab}}/\upsilon$
Re_Θ	=	Reynolds number based on the momentum thickness
S	=	spacing between two tab axes (in terms of h_{tab})
U, u'	=	streamwise mean and the corresponding rms velocities
U_r	=	reference mean velocity, $(U_1+U_2)/2$
U_s	=	secondary mean velocity, $\sqrt{(V^2+W^2)}$
U_1, U_2	=	mean velocity of the top and bottom streams
$u'v'$, $u'w'$, $v'w'$	=	Reynolds shear stresses
V, v'	=	vertical mean and the corresponding rms velocities
W, w'	=	horizontal mean and the corresponding rms velocities
x, y, z	=	streamwise, horizontal, and vertical directions
Γ_s	=	streamwise circulation per vortical structure
δ^*	=	displacement thickness, mm
Θ	=	momentum thickness, mm
θ	=	shear-layer entrainment momentum thickness, mm; subscript 0 indicates values at the trailing edge
υ	=	kinematic viscosity
Ω_x	=	streamwise vorticity, $(\partial W/\partial y)-(\partial V/\partial z)$

I. Introduction

STREAMWISE vorticity has long been recognized as one of the most efficient means to enhance turbulent mixing[1,2] and convective heat transfer.[3,4] Depending on applications, these two features acting together may or may not always be beneficial. In the case of the turbofan engine combustor where the vigorous mixing between the fuel and air is desirable, the corresponding increase in heat transfer to the surroundings has no advantage. However, in the case of turbofan engine exhausts vigorous mixing (between the core and bypassed flows so as to reduce the noise and enhance the thrust) and the augmented heat transfer to the surroundings (to reduce the thermal signature) are both desirable features. Thus, the investigations on the mechanisms of formation and evolution of the streamwise vorticity are of great importance to the effective operation of the aforementioned applications. Any possible interactions between the streamwise vortices and the Kelvin–Helmholtz-type vortices are of equal significance. As shown in the measurements of McCormick and Bennett[5] and Yu and Yip[6] on a lobed mixer (i.e., a convoluted splitter plate), the interactions of these two vortices produced the desired mixing enhancement.

Many different types of streamwise vortex-generating devices[7,8] had been tested in the past for their applications in turbofan engine exhausts and ejectors. In particular, the lobed mixers were successfully tested and implemented subsequently in some of the modern day aircraft engines. Typical examples include RR RB211 and F110-GE-100. In the case of fighter aircraft, the installation of the lobed mixer had significantly reduced the length of the afterburner and thereby the overall weight of the engine. Moreover, it is obvious that if the size of the lobed mixer can be reduced further the benefits arising from the improvement in thrust-to-weight ratio are enormous. This is particularly true in the case of fighter aircrafts where the key performance parameters such as maneuverability and supercruise will benefit tremendously from a lower thrust-to-weight ratio. The vortex-generating tabs, which are only small protrusions into the flows, have been shown to generate streamwise vortices of comparable strength (in terms of peak streamwise vorticity strength) to that of a lobed mixer.

Extensive experimental investigations on the tabs have been conducted in the past particularly in the area of jet flow. The works of Samimy et al.,[9] Zaman et al.,[10] and Reeder and Samimy[11] have provided many great detailed as well as subtle features into the effects of tabs in jet flow. Two sources for the generation of streamwise vorticity behind the tab have been identified (see Bohl and Foss[12] for a summary). The dominant source (denoted as 1) comes from the pressure hill formed upstream of the tab. The flow deceleration by the tab creates a pressure hill that, together with the presence of the wall, produces the pair of counter-rotating vortices. The mechanism is described mathematically by the Navier–Stokes equation applied at the wall:

$$\left.\frac{1}{\rho}\frac{\partial p}{\partial z}\right|_{y=0} = \left.\upsilon\frac{\partial(\Omega_x)}{\partial y}\right|_{y=0} \tag{1}$$

The second source (denoted as 2), again owing to the pressure gradients on the tab's surface, is the vortex shed from the sides of the tab.

Received 12 November 1999; accepted for publication 17 November 2000.

*Associate Professor, Thermal and Fluids Engineering Division, School of Mechanical and Production Engineering. Member AIAA.

†Research Student, Thermal and Fluids Engineering Division, School of Mechanical and Production Engineering.

Vortex is formed as the flow goes past the tab edge. As it convects downstream, it is reoriented by the velocity gradients in the shear layer to become streamwise vortex. If the approaching boundary layer upstream of the tab is thick, an additional vortex pair rotating in the opposite sense as the main pair would be developed and is consistent with the horseshoe vortex system. The most optimal tab shape should be triangular and must be attached firmly to the jet exit without gap.[9,10] A small gap of about half of the tab height can significantly reduce the effectiveness in streamwise vortices generation as a result of the disassociation of the pressure hill upstream of the triangular tab, which in turn reduces the contribution of source 1 just mentioned.

In the light of the achievements made by the aforementioned researchers, it may be worthwhile to examine the effects of the tabs in a two-stream mixing flow situation, i.e., in an environment similar to that encountered in the turbofan exhausts. With the exception of Foss and Zaman,[13] almost all of the previous investigations concerning tabs were in free or confined jets discharging to the quiescent surroundings. Hence, there is a lack of study on the effects of tabs in a two-stream mixing layer. This certainly motivates the present investigation. The present work attempts to advance the understanding of the effect of delta tabs downstream of a two-flowing stream separated by a partition. The tabs considered are of triangular shape with their apex tilted downstream at ±45 deg relative to the main flow direction. Previous experiments had shown that the tab effect was nominally the same in supersonic and subsonic flows indicating the tab jet phenomenon was independent of compressibility. Hence, the present experiments were conducted in a low-speed wind tunnel using a laser Doppler anemometer so as to provide detailed velocity measurements for the analyses of the flows.

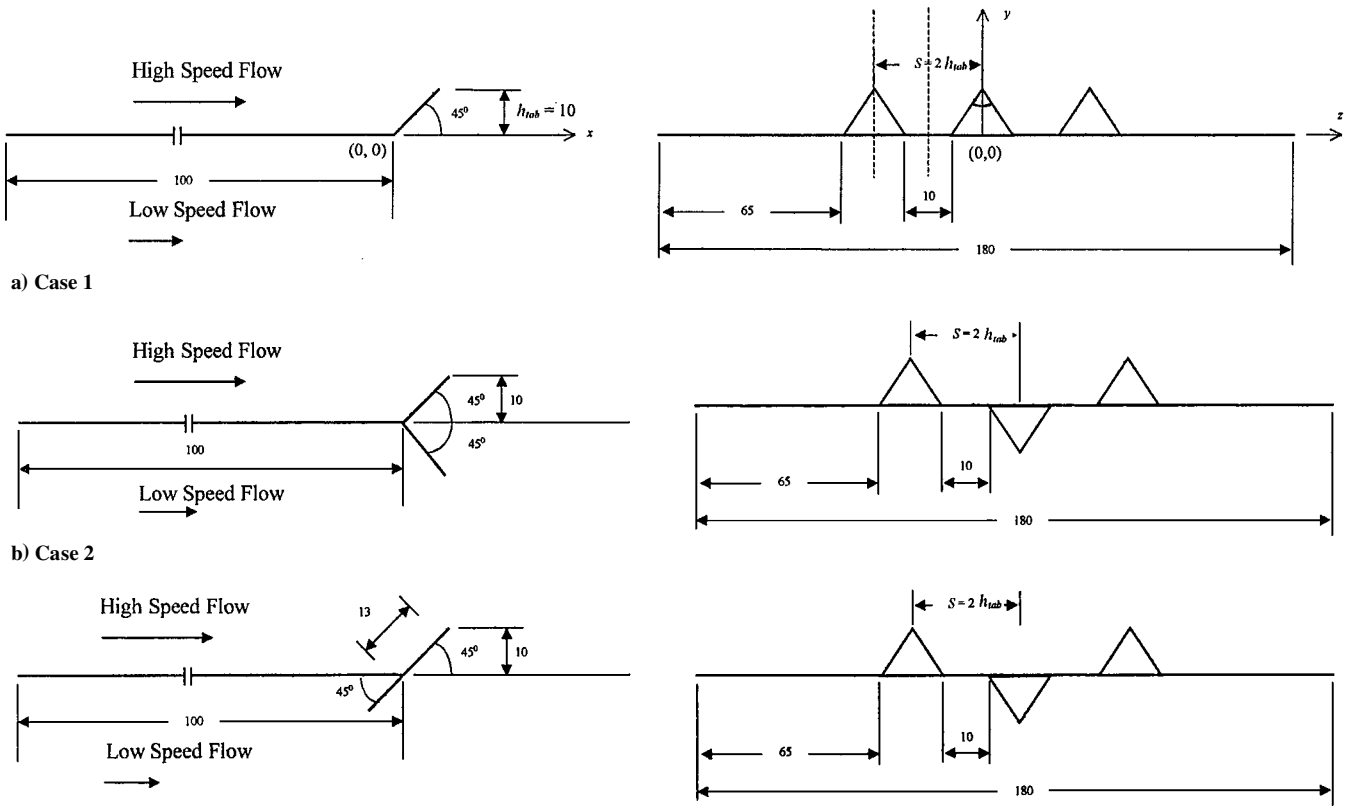

Fig. 1 Schematic of the multiple tab arrangement. (All dimensions are in millimeters.)

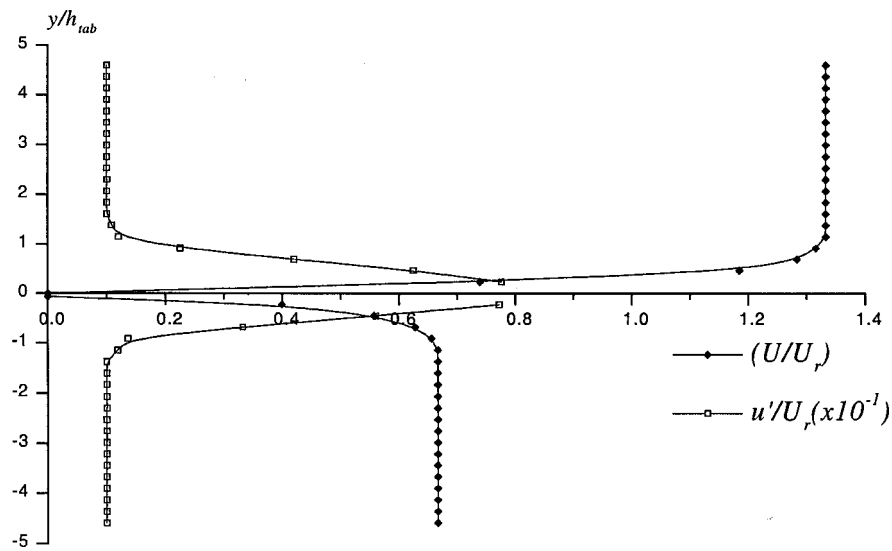

Fig. 2 Profiles of the normalized streamwise mean velocities U/U_r and the corresponding rms velocities u'/U_r at $10h_{tab}$ upstream of tab base.

The wind tunnel and the initial conditions are described in the next section and are followed by the instrumentation. The results are presented and discussed in Sec. III, and this paper ends with a summary of more important findings in Sec. IV.

II. Experimental Rigs and Instrumentation

A. Wind-Tunnel Facilities and Tab Configurations

The wind tunnel used for velocity measurements in the present investigation was similar to that used by Yu and Yip,[6] i.e., with a longer splitter plate extended to the entrance of the contraction section so that the contraction section was divided equally into two halves. The arrangement was to ensure relatively low freestream turbulence levels (< 1% of the local mean velocity) on entry to the test section on either side of the splitter plate. The plexiglass test section was 200 mm high, 200 mm wide, and 500 mm long. Different velocity ratios between the upper and lower streams were achieved by incorporating cloth and wire meshes on the lower half of the contraction section. The speed range of the wind tunnel, in the absence of the splitter plate, could be varied from 1 to 15 m/s. In the present investigation a mean speed of 7.5 m/s was used, which corresponded to a Reynolds number of 5.128×10^3 (based on the projected height of the tab at 10 mm).

Figure 1 shows general sketches of the tab configuration employed in the present work, i.e., the "inverted delta tab," which is triangular with its tip angled downstream. Detailed dimensions are given in the figure. The tab base was attached to the trailing edge and at the center of the splitter plate so that no gap existed between the tab and the trailing edge. As shown in the preceding measurements,[10] a small gap equal to the width of the tab will drastically diminish its effect on the flow. Three arrangements for the tabs were used. Case 1 has all three tabs on the high-speed side. The second arrangement involves tabs placed alternatively on either side of the splitter plate. Case 3 is similar to case 2, but the tab on the low-speed side is tilted upstream (i.e., similar to a delta-win vortex generator).

B. Initial Conditions

The boundary-layer velocity profiles on either side of the splitter plate measured at $10h_{\text{tab}}$ upstream of the tab base (i.e., the trailing edge) had a thickness of about 9 mm (boundary-layer thickness defined at $0.99U_{\max}$); see Fig. 2. The calculated boundary-layer

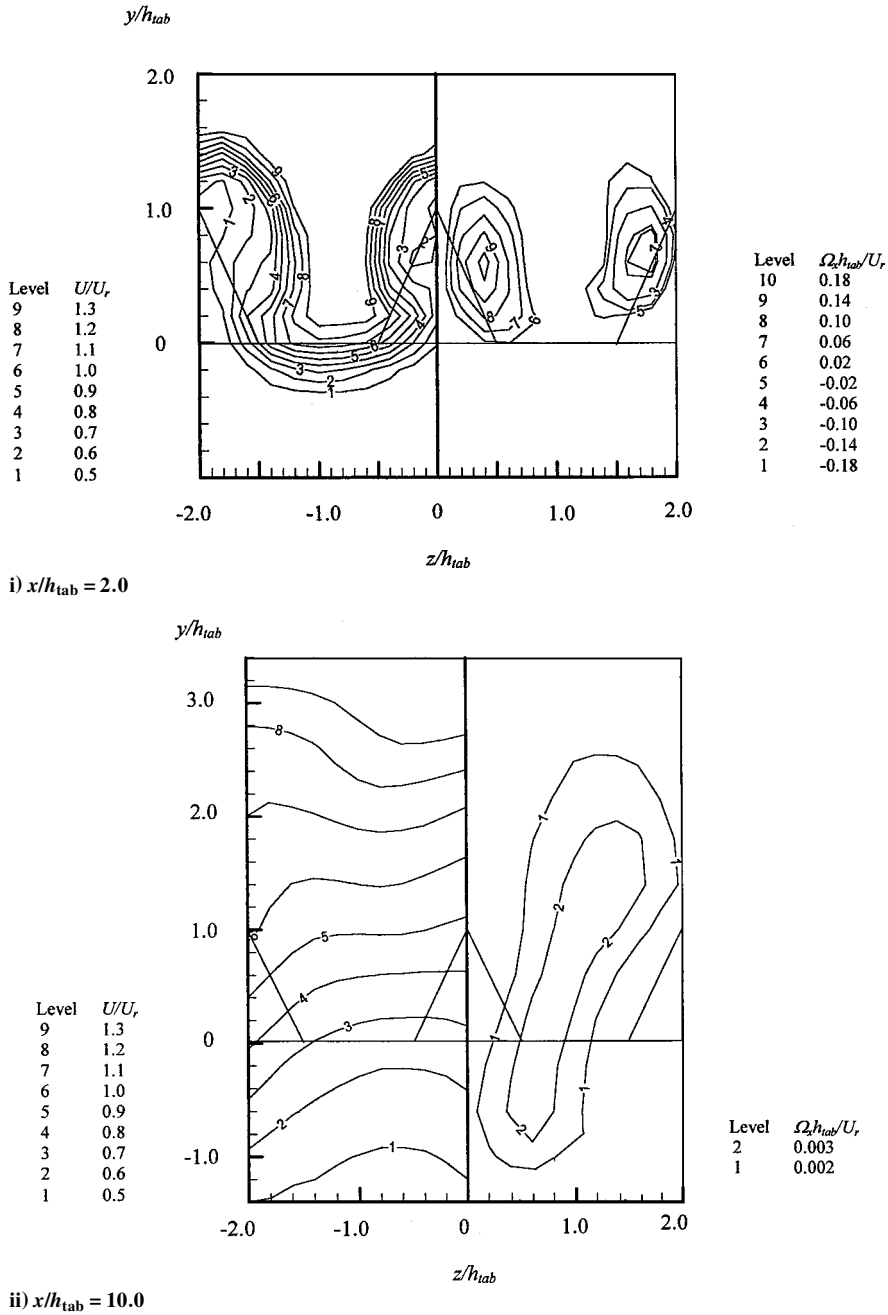

Fig. 3a Contours of normalized streamwise mean velocity U/U_r and the corresponding streamwise vorticity ($\Omega_x h_{\text{tab}}/U_r$) for case 1.

parameters are shown in Table 1. Both boundary-layer parameters and boundary-layer profiles indicated that the boundary layers on either side of the lobed mixer were turbulent. Streamwise turbulence level outside the boundary-layer region had maximum values of 1% (normalized by the mean velocity of the local stream) and rose to about 8% close to the surface of the splitter plate.

Table 1 Boundary-layer parameters at $10h_{tab}$ upstream of the penetration region

Stream	U, m/s	δ^*, mm	Θ, mm	H	Re_Θ
Top	10.0	0.52	0.391	1.33	269
Bottom	5.0	0.48	0.34	1.41	140

C. Laser Doppler Anemometer

A six-beam three-component fiber-optic laser Doppler anemometer (manufactured by TSI, Inc.) together with a 2-W argon ion laser operating in a backward scatter mode was used to measure respective velocity components. Two fiber-optic probes (TSI 9275-1) were used. The first one had a focusing lens of 400 mm, which provided a measuring probe volume of $0.09 \times 0.09 \times 1.31$ mm in the vertical direction y and $0.085 \times 0.085 \times 1.24$ mm in the streamwise direction x. For the horizontal direction z a probe volume of $0.083 \times 0.085 \times 1.22$ mm was formed from the second fiber-optic probe coupled with a 300-mm focusing lens. The two fiber-optic probes were mounted together on the same vertical bench attached to an automated three-dimensional traversing system (with an accuracy of ± 0.01 mm). The six laser beams were then projected to the same point inside the test section

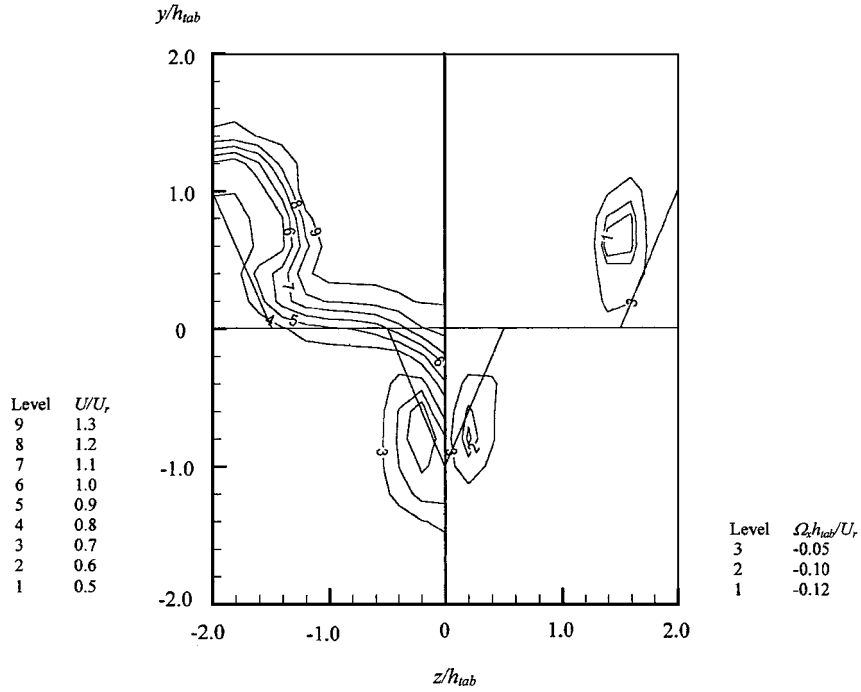

i) $x/h_{tab} = 2.0$

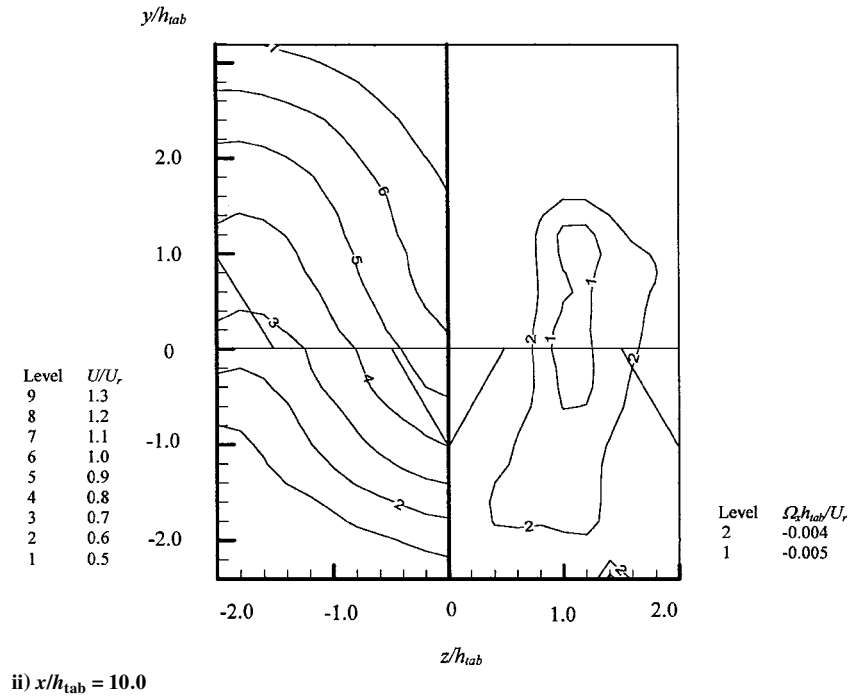

ii) $x/h_{tab} = 10.0$

Fig. 3b Contours of normalized streamwise mean velocity U/U_r and the corresponding streamwise vorticity $\Omega_x h_{tab}/U_r$ for case 2.

for measurements. Bragg shifting of frequency up to 2 MHz (on each channel) was used to avoid directional ambiguity. The Doppler signals were detected by photomultipliers (TSI 9162) and processed by the automatic burst correlators (TSI IFA 750). Fine water particles, sizes within 5–10 μm, generated by a commercial vaporizer were used to seed the flow. They were injected into the wind tunnel upstream of the settling chamber before the contraction section. Except at some regions immediately behind the trailing edge, data rates of 500–1000 Hz were normally obtainable. At each measuring point the mean velocities (U, V, and W), the rms of the velocity fluctuations (u', v', and w'), and the Reynolds shear stresses ($u'v'$, $u'w'$, and $v'w'$) were determined from population of more than 5000 (on each channel) independent samples together with a coincidence

Table 2 Summary of the experiments undertaken

Case	No. of tab	Velocity ratio (upper: lower)	Description
1	3	2:1	All of the tabs are on the high-speed side
2	3	2:1	High-speed flow on the side of two tabs and low-speed flow on the side of one tab
3	3	2:1	High-speed flow on the side of two tabs and low-speed flow on the side of one tab (tilted upstream)

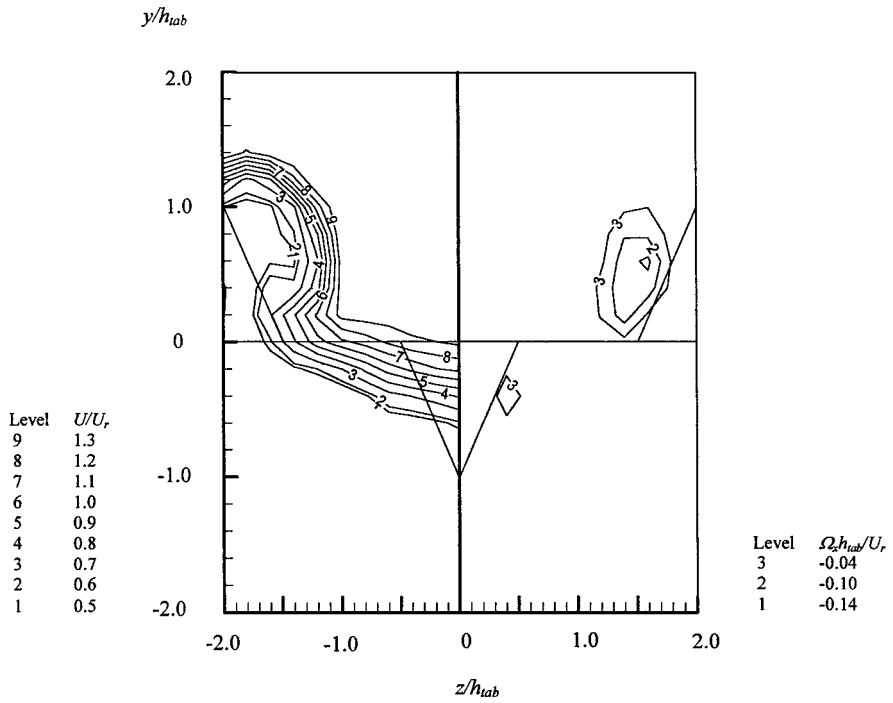

i) $x/h_{tab} = 2.0$

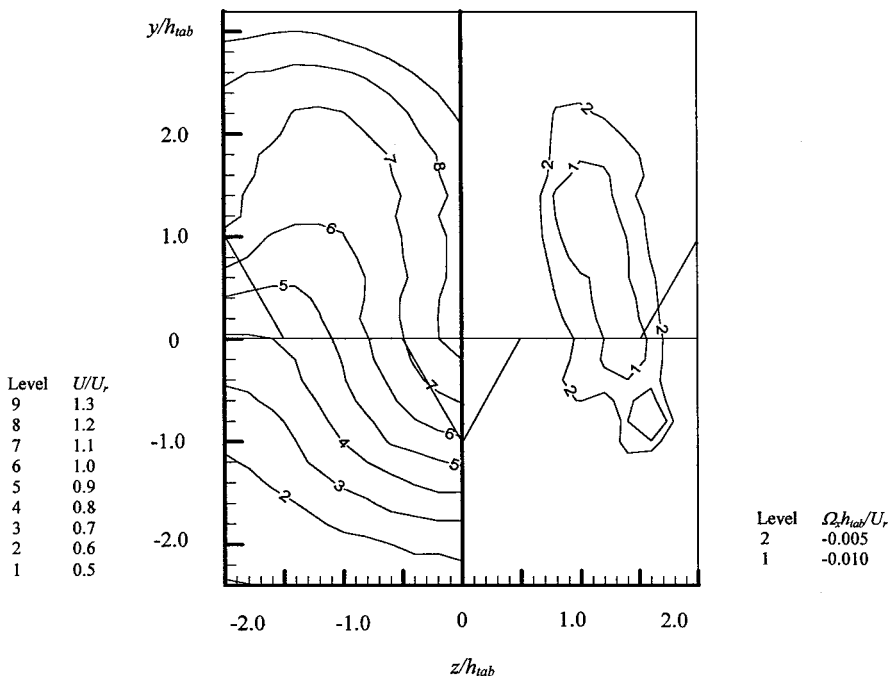

ii) $x/h_{tab} = 10.0$

Fig. 3c Contours of normalized streamwise mean velocity U/U_r and the corresponding streamwise vorticity $\Omega_x h_{tab}/U_r$ for case 3.

window of 1 μs via the software package (FIND) provided by TSI. The experiments were conducted in an air-conditioned room with the temperature of the air maintained at 25°C at all times.

A careful appraisal on the errors associated with the laser Doppler anemometry system was conducted. The sources of error were mainly stemmed from velocity biasing, velocity gradient broadening,[14] the accuracy of the signal processor, the finite sample size,[15] and multiple particles in the control volumes.[16] Accuracy of the measured velocity components U, V, and W (normalized by the bulk mean velocity of the two streams U_r) can be expected to be at about 2% and that of the rms of the velocity fluctuations u', v', and w' (normalized by U_r) are 5%. The Reynolds shear stresses $u'v'$, $u'w'$, and $v'w'$ (normalized by U_r^2) lie within the range of 10–20%.

Streamwise mean vorticity ($\Omega_x = \partial W/\partial y - \partial V/\partial z$) was evaluated using a cubic spline interpolation to the velocity measurements in the y and z directions. Results (based on a single tab) obtained became independent of grid density when Δz and Δy were both kept below $0.1h_{\text{tab}}$. The estimated accuracy of the streamwise mean vorticity is therefore expected to be within 25%.

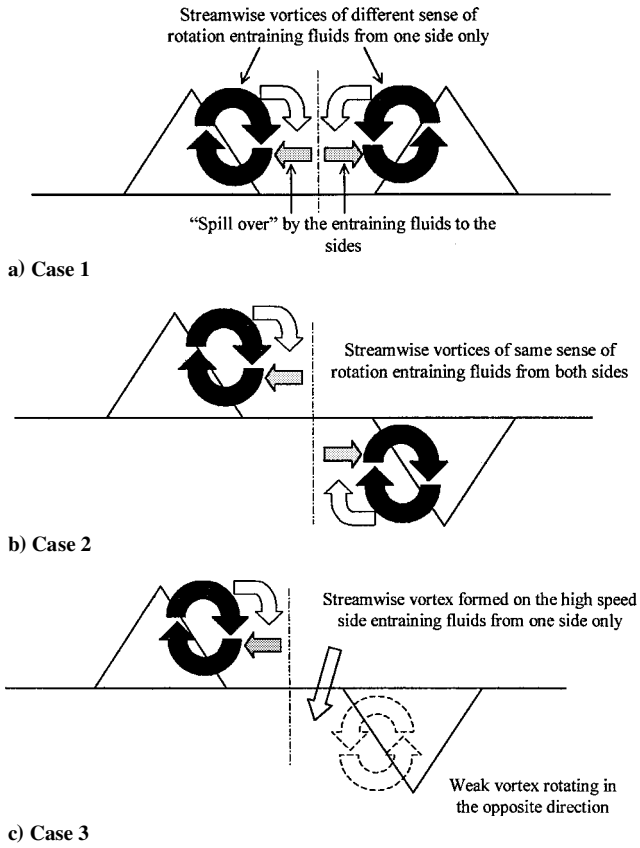

Fig. 4 Schematic of streamwise vortices distribution in the vicinity of the trailing edge for respective cases.

D. Experimental Procedures

Velocity measurements were acquired at $x/h_{\text{tab}} = 2$, 4, 6, 10, and 20, respectively. The upstream area had a total of 525 measuring points, and the downstream area had about 1023 points. The distance separating two measuring control volume locations was about $0.1h_{\text{tab}}$. Further details can be obtained from Koh.[17] Altogether three experiments have been conducted and are listed in Table 2.

III. Results and Discussion

A. Mean Quantities

The mean streamwise velocity contours U/U_r and the corresponding mean streamwise vorticity contours $\Omega_x h_{\text{tab}}/U_r$ at two representative stations within the range $x/h_{\text{tab}} = 2.0$–10.0 for each case are presented in Figs. 3a–3c. The results presented here are at spacing between two tabs' axes at $2h_{\text{tab}}$.

A sinusoidal-type spanwise distortion is evident at the first station for case 1, as may have been expected. The distortion of the contours is the direct result of the counter-rotating vortices generated behind each tab. Local maxima in the velocity defect were also found at regions between the two contrarotating vortices behind each tab. Farther downstream at $x/h_{\text{tab}} = 10.0$, the distortion became less severe, but the spanwise sinusoidal variation persisted albeit with a different wavelength. The development of the mean velocity contours suggests that the spanwise wavelength of the original distortion is not maintained with streamwise distance, implying that the spacing of the streamwise vortices is also not maintained, i.e., interactions between neighboring vortices would have taken place. The corresponding vorticity plot clearly shows that the vorticity decays rapidly in strength with downstream distance from a peak level of 0.14 at $x/h_{\text{tab}} = 2.0$ to 0.003 at $x/h_{\text{tab}} = 10.0$.

Figure 3b shows the corresponding development for case 2. Similar to that of case 1, the distortion of the contours behind the tabs on the high-speed side is also apparent. The tab on the low-speed side acts as an attachment surface for the flow from the high side to

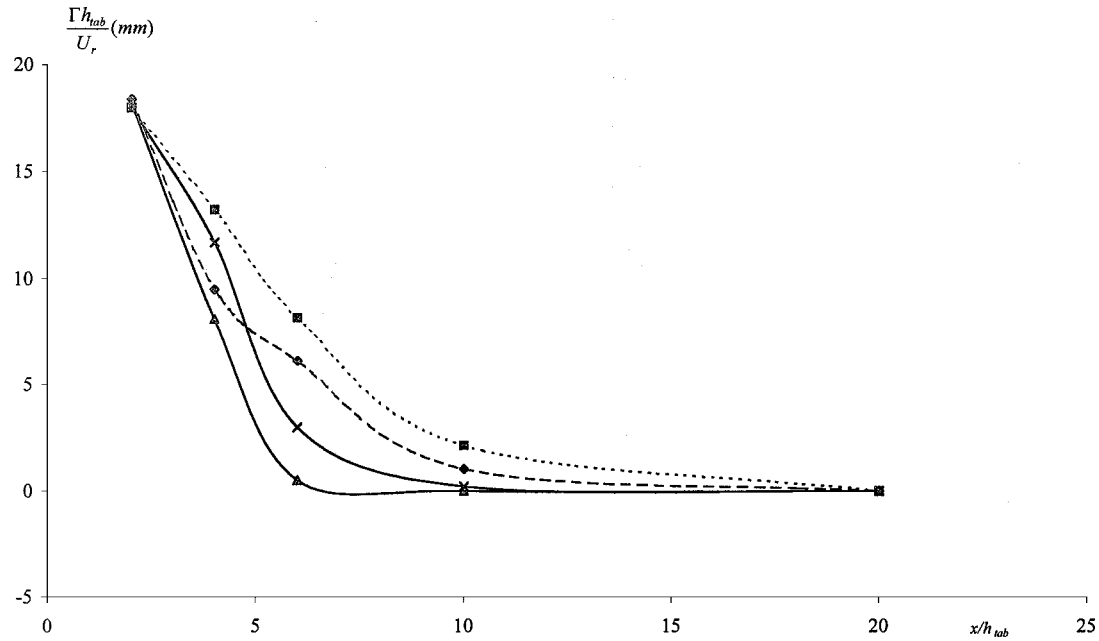

Fig. 5a Streamwise development of average circulation (on the streamwise vortex on the high-speed side) for respective cases: ◆, case 1; ■, case 2; ▲, case 3; and ×, single tab.

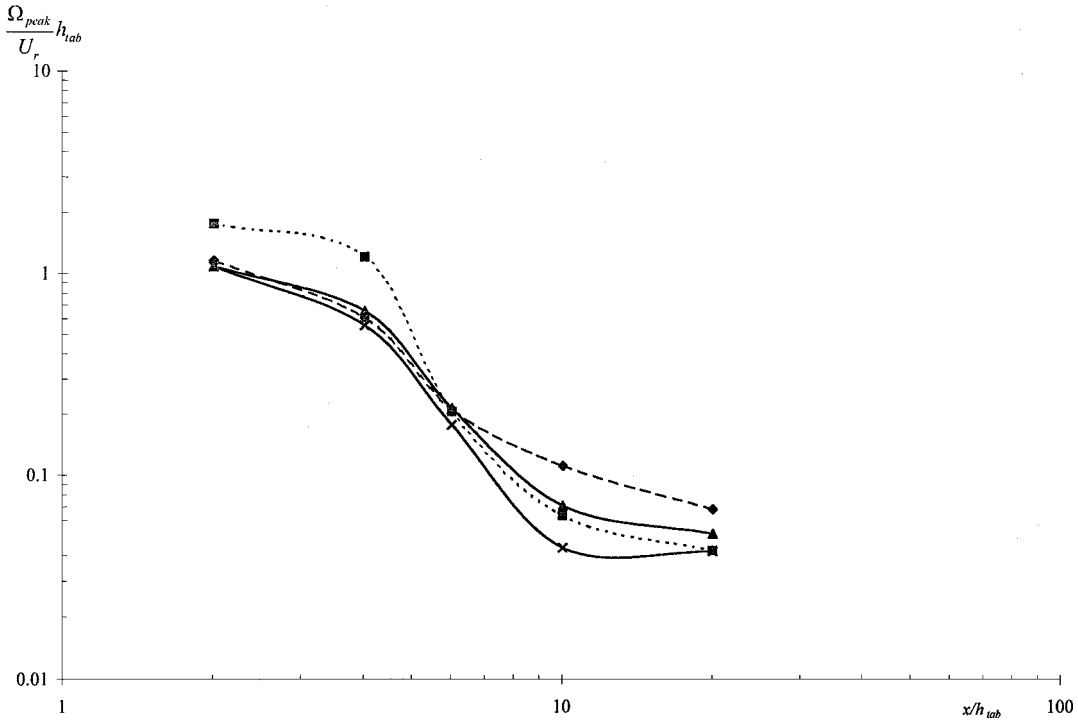

Fig. 5b Streamwise development of peak mean streamwise vorticity for respective cases: ◆, case 1; ■, case 2; ▲, case 3; and ×, single tab.

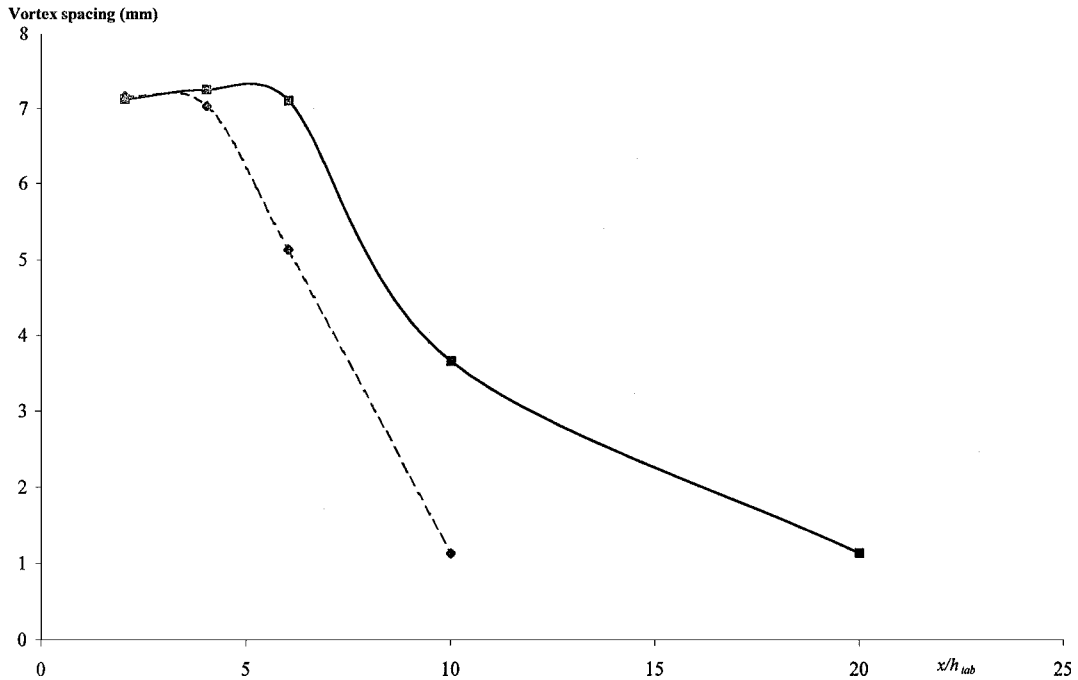

Fig. 5c Streamwise development of vortex spacing for cases 1 and 2: ◆, case 1; and ■, case 2.

penetrate into the low-speed side.[13] A pair of contrarotating vortices is also formed behind each tab. As may be expected, a higher level of streamwise vorticity is found on the higher speed side. The sense of rotation for the two vortices between the two tab axes is the same. At a station farther downstream the distortion of the contour persists, and the same shape is maintained. The distance between any two contour levels is more widely spaced indicating the effects of diffusion. The vorticity contours provide some interesting results. From $x/h_{\text{tab}} = 2.0$ to $x/h_{\text{tab}} = 10.0$, the merging of two vortices into one is observed, and the level of vorticity is generally decreased with downstream distance. For case 2 the decay of the vorticity is not as rapid as case 1, and the peak vorticity level decays from 0.15 at $x/h_{\text{tab}} = 2.0$ to 0.005 at $x/h_{\text{tab}} = 10.0$.

The flow development for case 3 is shown in Fig. 3c. The distortion of the contours in general is very similar to that found in case 2, but the penetration of the flow from the high-speed side to the low-speed side is less pronounced in this case as a result of the absence of the attachment surface. The distortion of the contours on the high-speed side is, however, similar to that found in cases 1 and 2. The corresponding vorticity plot shows only the formation of streamwise vortices on the high-speed side but not on the low-speed side. The vortices generated on the low-speed side by the upstream tilted tab should have strength much lower than that generated on the high-speed side, which also are of an opposite sense of rotation. It is therefore likely that the weaker vortex may have been canceled out by the stronger vortex. The decay of peak vorticity level with

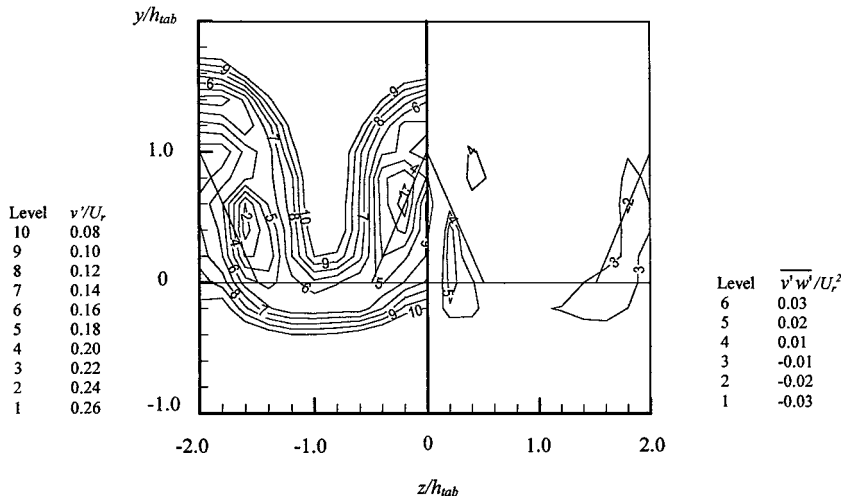

Fig. 6a Contours of the normalized vertical component of fluctuations v'/U_r and the corresponding Reynolds shear stress $\overline{v'w'}/U_r^2$ for case 1 at $x/h_{tab} = 2.0$.

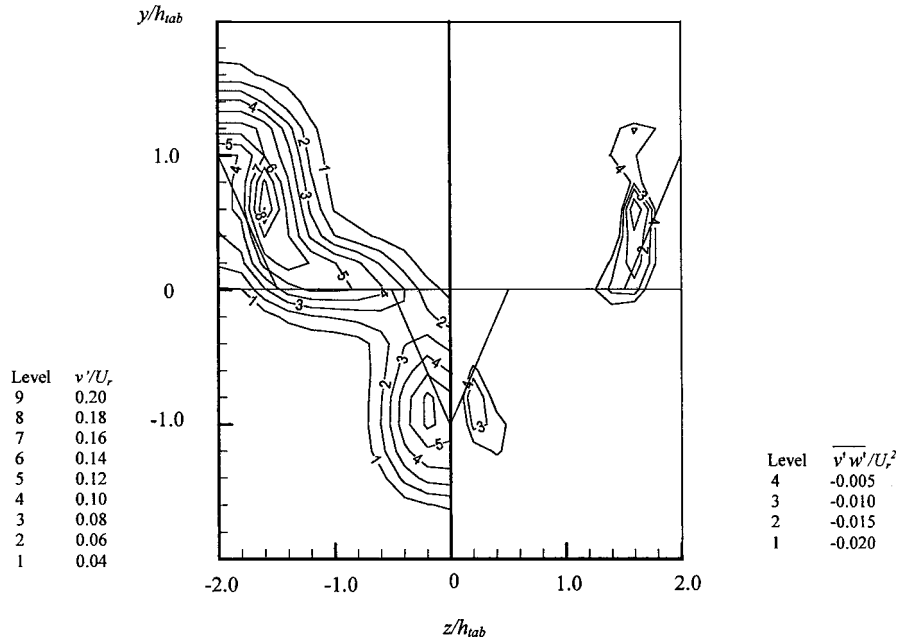

Fig. 6b Contours of the normalized vertical component of fluctuations v'/U_r and the corresponding Reynolds shear stress $\overline{v'w'}/U_r^2$ for case 2 at $x/h_{tab} = 2.0$.

downstream distance is also found to be faster than case 1 but similar to case 2, i.e., from a level of 0.14 at $x/h_{tab} = 2.0$ to 0.005 at $x/h_{tab} = 10.0$.

Based on the results just obtained, schematic views on the distribution of the streamwise vortices near the trailing edge can be constructed and are shown in Figs. 4a–4c for the three cases, respectively. Case 1 consists of two counter-rotating vortices between two tab axes. The vortices are actually entraining the surrounding fluids toward the central axis. However, at stations farther downstream the two streamwise vortices would be diffused, and mutual cancellations would have occurred; this may cause the slowdown in the entrainment growth rate after $x/h_{tab} = 4.0$. Similarly for case 2 in Fig. 4b, the two streamwise vortices are actually rotating in the same sense, and they convect the surrounding fluids toward the central axis from both sides of the partition. At locations farther away from the trailing edge, the two vortices diffused and merged into one. For case 3 the relatively weaker vortex on the low-speed side was canceled out by the stronger vortex immediately after the trailing edge. The growth rate along the two tab axes may also be enhanced, which could be caused by the "spill over" of the entrained fluids from the central axis to the tab axes, as indicated in Fig. 4.

B. Downstream Development of the Streamwise Vortices

To examine the evolution of the mean streamwise vorticity in a more quantitative manner, the streamwise development the average circulation, the peak mean streamwise vorticity, and vortex spacing are plotted in Figs. 5a–5c, respectively. All of the parameters just mentioned are obtained at the region between two tab axes. It will be shown later that the single tab characteristics can be modified tremendously when several tabs are arranged in an array.

The streamwise evolution of the average circulation per vortical structure (only on the higher strength vortex on the high-speed side) is presented in Fig. 5a. The circulation was determined by obtaining the surface integral of the streamwise vorticity region. The average circulation near the trailing edge is similar for all cases including the single tab case. However, the decay for case 3 and the single tab case is very rapid, i.e., the vortex decays faster when there is no or little interaction with the neighboring vortex. In contrast, the decay rates for the other two cases (1 and 2) are more gradual with case 2 providing the lowest decay rate. If we recall the development of streamwise vorticty contours in Fig. 3, one possible reason for the faster decay in case 1 may be caused by the cancellation of the streamwise vortices of opposite signs. Similarly,

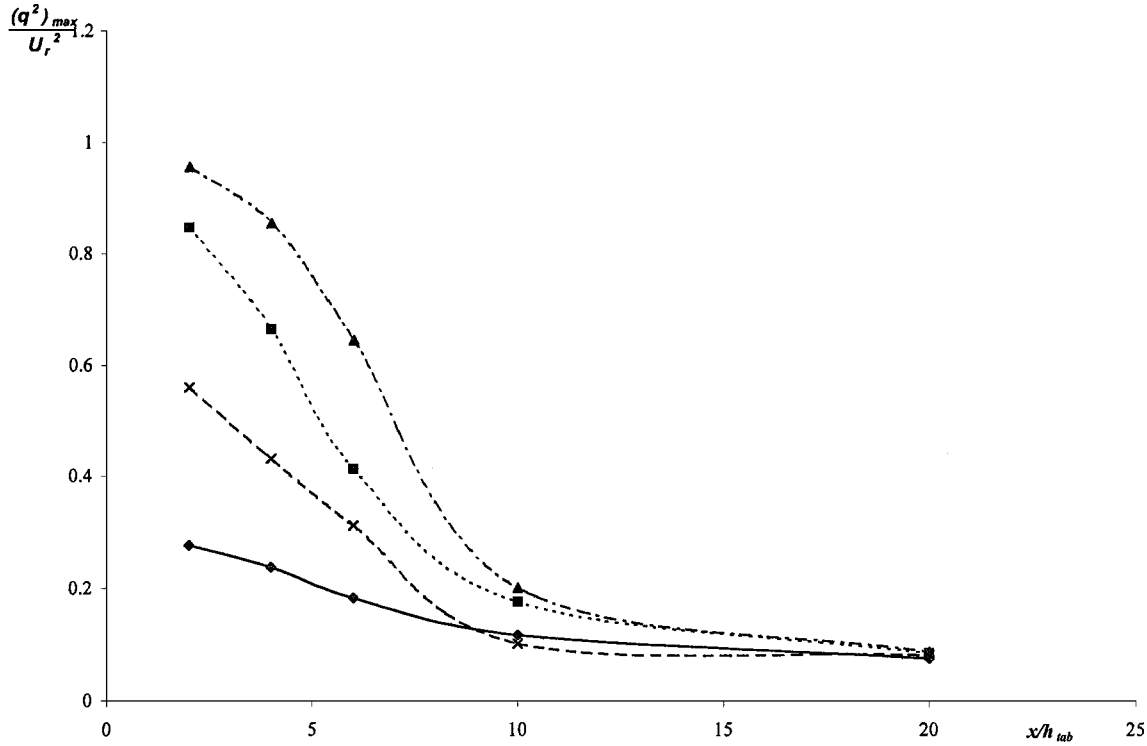

Fig. 7 Streamwise development of peak turbulent kinetic energy for respective cases: ◆, planar; ■, case 1; ▲, case 2; and ×, case 3.

for case 2 the slower decay can be attributed to the merging of the streamwise vortices of the same signs (cf., Fig. 3b). For case 3 the decaying pattern is very much the same as that of a single tab before $x/h_{tab} = 10.0$, indicating the vortex generated by the upstream tilted tab on the low-speed side has no direct effect on the overall development of the streamwise vorticity.

The development of the peak mean streamwise vorticity in Fig. 5b is plotted on a log-log scale. Results for all cases considered here appear to fall on the same decaying curve, and an obvious decreasing trend persists through the range of measurement. The peak level reduces to an almost negligible level after $x/h_{tab} = 10.0$. The decaying pattern is also similar to that of a single tab. The maximum peak streamwise vorticity level for the tab on the high-speed side is 7% lower than the level obtained by Foss and Zaman.[13] This may be attributed to the difference in the geometry of the tab considered by them had a wider base (in their case the tab base was $2h_{tab}$ comparing to $1h_{tab}$ in the present case).

The development of the mean spacing of the streamwise vortical structures, calculated by the estimated distance of the cores between two adjacent vortices between two tab axes, is shown in Fig. 5c. In case 1 the spacing is maintained until after $x/h_{tab} = 4.0$, whereas that of case 2 reduces sharply at around $x/h_{tab} = 6.0$. An irregular spanwise distribution clearly suggested mechanisms such as vortex merging and mutual cancellation have taken place. This may also explain the fast decay for the streamwise vorticity and the average circulation observed earlier in Figs. 5a and 5b.

C. Turbulence Quantities

The distributions of the turbulence quantities at the downstream stations are also affected by the generation of the steamwise vorticity. The effects of the Reynolds stresses are qualitatively similar, i.e., each tends to transport momentum from a high-velocity to a low-velocity region, and the vortices tend to rotate fluid about the x axis. Of particular interest is the distribution on the generation of the fluctuation components in the lateral directions. As shown in Figs. 6a and 6b, the distribution of the v' fluctuating velocity components for cases 1 and 2. The regions of maximum magnitude coincide with the maximum streamwise vorticity. This is not too surprising if one considers the production terms $v'w'(\partial V/\partial z)$ for the v' fluctuating velocity components [and $v'w'(\partial W/\partial y)$ for the w' fluctuating velocity components) in which the gradients of traverse velocity components contribute partly to the streamwise vorticity ($\Omega_x = \partial W/\partial y - \partial V/\partial z$). The corresponding distributions for the contours of $v'w'$ are shown in Figs. 6a and 6b. As is clearly shown from Figs. 4 and 5, $v'w'$ and $\partial V/\partial z$ are of the opposite sign signifying a positive contribution to the fluctuating components. The measurements of Foss and Zaman[13] had indicated that strong dissipation also appears at a region close to the peak streamwise vorticity. As a result of the imbalance of the turbulence production and dissipation, the diffusion terms $\partial v'^3/\partial y$ and $\partial w'^3/\partial z$ should be decreasing slowly away from the vortex cores, indicating that diffusion effects are important at the stations farther downstream. This would eventually lead to the smoothing out of the mean velocity gradients across the shear layers.

The fluctuation intensity results can be combined to represent the turbulence kinetic energy, i.e., $\overline{q^2}/2 = [\overline{u'^2} + \overline{v'^2} + \overline{w'^2}/2]$. The streamwise development of the maximum turbulent kinetic energy within the wake is shown in Fig. 7. The peak generally appeared at locations closer to the trailing edge. The highest level is found to be in case 2, and it is followed by cases 1 and 3, and finally the planar case. The high turbulence levels at regions close to the trailing edge are attributed to additional production caused by the mean velocity gradients of all three mean velocities generated within the wake. The level for each case however drops rapidly after $x/h_{tab} = 6.0$, and they asymptote to lower levels at further downstream stations.

IV. Summary

An experimental investigation was conducted on three tab array arrangements at a velocity ratio of 2:1. The vortex-generating tabs are in the form of delta tabs, triangular-shaped protrusions into the flow, attached to the trailing edge of the splitter plate. The first case had all of the tabs located on the higher-speed side, and the second and third case had the tabs located alternatively on either side of the splitter plate. For case 3 the tab on the low-speed side was tilted upstream (i.e., similar to a delta-wing vortex generator).

As may have been expected, distortion on the wake was observed for the three cases immediately after the trailing edge. At a given tab spacing (i.e., $2h_{tab}$ in the present investigation) the effects of the streamwise vortex array would have generally facilitated the mass flux entrainment rate and enhanced the level of turbulence for mixing. The wavelength of the distortion however was not maintained because of the interactions between neighboring vortices at

a short distance downstream of the trailing edge. Depending on the tab arrangements, mutual cancellation between streamwise vortices rotating in the opposite sense was observed in case 1, whereas in case 2 the merging of streamwise vortices rotating in the same sense had delayed the decay of the streamwise vorticity. For case 3 the upstream tilted tab appeared to have generated relatively weak streamwise vortices so that they were canceled by the vortices generated on the high-speed side near the trailing edge. The expected benefits arising from the arrangement in case 3, in terms of entrainment rate and elevated turbulence level, were therefore marginal, compared to that of the other two cases and a single delta tab case.

Acknowledgments

Financial support to this project from the Academic Research Fund and the graduate scholarship for P. K. Koh from the School of Mechanical and Production Engineering at Nanyang Technical University are gratefully acknowledged.

References

[1]Bradbury, L. J. S., and Khadem, A. H., "The Distortion of a Jet by Tabs," *Journal of Fluid Mechanics*, Vol. 70, 1975, pp. 801–813.

[2]Gretta, W. J., and Smith, C. R., "The Flow Structure and Statistics of a Passive Mixing Tab," *Journal of Fluids Engineering*, Vol. 115, 1993, pp. 255–263.

[3]Sanger, J. L., and Dellenback, P. A., "Heat Transfer in Counterswirled Coaxial Jet Mixing," *Journal of Propulsion and Power*, Vol. 14, No. 3, 1998, pp. 384–391.

[4]Khodadadi, J. M., and Vlachos, N. S., "Experimental and Numerical Study of Confined Coaxial Turbulent Jets," *AIAA Journal*, Vol. 27, No. 5, 1989, pp. 532–541.

[5]McCormick, D. C., and Bennett, J. C., Jr., "Vortical and Turbulent Structure of a Lobed Forced Mixer Free-Shear Layer," *AIAA Journal*, Vol. 32, No. 9, 1994, pp. 1852–1859.

[6]Yu, S. C. M., and Yip, T. H., "Measurements of Velocities in the Near Field of a Lobed Forced Mixer Trailing Edge," *Aeronautical Journal of the Royal Aeronautical Society*, Vol. 101, March 1997, pp. 121–129.

[7]Barber, T., Paterson, R. W., and Skebe, S. A., "Turbofan Forced Mixer Lobe Flow Modeling Vol. 1: Experimental and Analytical Assessment," NASA CR4147, 1988.

[8]Zaman, K. B. M. Q., "Streamwise Vorticity Generation and Mixing Enhancement in Free Jets by 'Delta-Tabs," AIAA Paper 93-3253, 1993.

[9]Samimy, M., Zaman, K. B. M. Q., and Reeder, M. F., "Effect of Tabs on the Flow and Noise Field of an Axisymmetric Jet," *AIAA Journal*, Vol. 31, 1993, pp. 609–619.

[10]Zaman, K. B. M. Q., Reeder, M. F., and Samimy, M., "Control of an Axisymmetric Jet Using Vortex Generators," *Physics of Fluids*, Vol. 6, No. 2, 1994, pp. 778–793.

[11]Reeder, M. F., and Samimy, M., "The Evolution of a Jet with Vortex-Generating Tabs: Real Time Visualization and Quantitative Measurements," *Journal of Fluid Mechanics*, Vol. 331, 1996, pp. 73–118.

[12]Bohl, D., and Foss, J. F., "Near Exit Plane Effects Caused by Primary and Primary-Plus-Secondary Tabs," *AIAA Journal*, Vol. 37, No. 2, 1999, pp. 192–201.

[13]Foss, J. K. F., and Zaman, K. B. M. Q., "Large and Small Scale Vortical Motions in a Shear Layer Perturbed by Tabs," *Journal of Fluid Mechanics*, Vol. 382, 1999, pp. 307–329.

[14]Durst, F., Melling, A., and Whitelaw, J. H., *Principles and Practice of Laser-Doppler Anemometry*, Academic Press, London, 1981.

[15]Yanta, W. J., and Smith, R., "A.Measurements of Turbulence Transport Properties with a Laser-Doppler Velocimeter," AIAA Paper 73–169, 1973.

[16]Driver, D. M., and Hebbar, S. K., "Experimental Study of a Three Dimensional, Shear Driven Turbulent Boundary Layer," *AIAA Journal*, Vol. 25, 1987, pp. 35–42.

[17]Koh, P. K., "Experimental Studies of Two-Stream Mixing Flows with Vortex-Generating Tabs," M.Eng. Thesis, Thermal and Fluids Engineering Div., School of Mechanical and Production Engineering, Nanyang Technological Univ., Singapore, 2000.

M. Samimy
Associate Editor